A computational study of the behavior of colloidal gel networks at low volume fraction

Hamed Hatami-Marbini [ID]

Mechanical and Industrial Engineering Department, University of Illinois at Chicago, Chicago IL, United States of America

E-mail: hatami@uic.edu

CrossMark

Abstract

Colloidal gel networks appear in different scientific and industrial applications because of their unique properties. Molecular dynamics simulations could reveal the relation between molecular level and macroscopic properties of these systems. Nevertheless, the predictions of numerical simulations might depend on the specific form and parameters of interaction potentials. In this paper, a new effective interaction potential is used for characterizing the mechanical behavior of low volume fraction colloidal gels under large shear deformation. The findings are compared with those obtained from other available forms of interaction potentials in order to determine gel characteristics that are interaction potential independent. Furthermore, the macroscopic stress–strain behavior is discussed in terms of the behavior of different terms of the proposed interaction potential. The correlation between the stretch of interparticle bonds and their alignment in the direction of the maximum principal stress is also computed in order to provide microscopic explanations for the initial strain softening behavior. It is concluded that, in addition to topology, local mechanical interactions between colloidal particles are important in defining the mechanical response of soft gels.

Keywords: colloidal gel networks, molecular dynamics, interaction potentials, mechanical properties, strain softening, large deformation

(Some figures may appear in colour only in the online journal)

Introduction

The interactions between microscopic particles forming colloidal suspensions give rise to unique physical behaviors. Such systems are ubiquitous in nature and find applications in different biology, cosmetics, and food technologies. They are also of particular interest for a range of smart materials as their properties can be tuned by nanofabrication of colloidal particles to produce desired mechanical behaviors and microstructures in a finely controlled way [1–8]. The unique and striking physical features of colloidal systems are also of significant importance for the fundamental understanding of the condensed soft matter [9, 10]. Among such features is their

ability to form soft gels: metastable spanning arrested network structures that could resist mechanical stress.

Gelation is a complex thermodynamic and kinetic process that depends on the volume fraction and the specific form of interparticle interactions. At high volume fractions, an amorphous solid can be formed because of jamming and crowding of colloidal particles. With decreasing the volume fraction, gels and network structures start to form. The gelation process has been explained via several mechanisms such as phase separation, glass-like kinetic arrest, percolation, and/or formation of locally favored structures [11–14]. At low volume fractions ($\phi < 15\%$), colloidal particles form gels by aggregating into fractal clusters as a result of spinodal decomposition
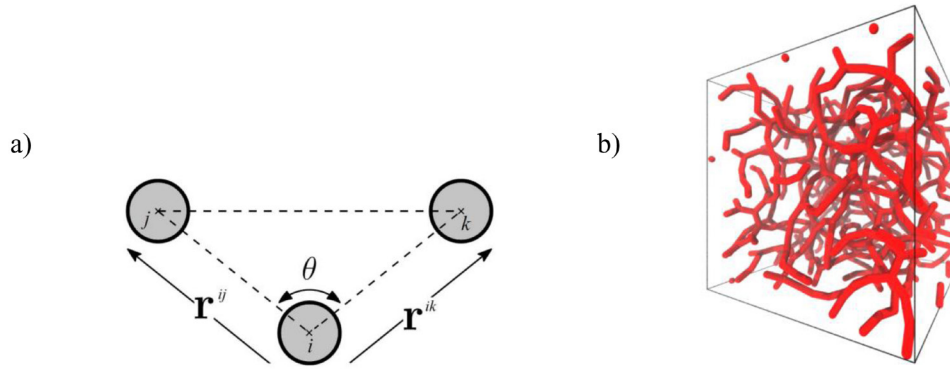
Figure 1. (a) Three interacting particles forming a bond angle θ, (b) typical get networks obtained using the present model at $\phi = 0.05$.

and diffusion-limited aggregation [15]. Experimental studies using confocal microscopy showed that gels at low volume fractions are indeed open connected clusters composed of chains of colloidal particles, which can resist bending deformations [16–19].

Computer simulations of colloidal gels could be used to better understand their microstructural and mechanical characteristics. The potentials that are used to represent the interaction between colloidal particles are expected to affect the predictions of these numerical studies. For example, numerical models using centrosymmetric effective interactions have successfully reproduced experimentally observed behavior of gels at moderate volume fraction such as the aggregation of particles into spanning clusters [20, 21]. Nevertheless, these models tend to undergo phase separation at low volume fraction rather than forming stable gel networks, which are observed experimentally. Open gel structures will be obtained if anisotropic effective interactions are introduced using dipolar, patchy or maximum-valence particles, or repulsive many-body interactions [22–30].

In addition to their microstructure, the nonlinear mechanical response of gels has been studied numerically [31, 32]. These previous numerical studies have provided valuable insight into the origin of complex mechanical response of gels and its relation to their topology. However, these recent results have been obtained with only one specific type of many body potentials [31, 32]. This particular form of interaction potential has been written using one convenient set of parameters in order to facilitate gelation under isothermal conditions and capture important physical aspects of colloidal gels. It is known that the mechanical behavior of gels strongly depends on their microstructure and physical processes occurring at small length scales [9]. Thus, possible effects of different forms of interaction potentials on the mechanics of gels should be addressed. In other words, it is important to investigate whether other forms of many body potentials could result in similar network structures at low volume fractions and whether the numerical predictions for the mechanical response of such colloidal gels depend on the ad hoc selection of the potentials.

In this paper, we focus on the relationship between potential interactions of colloidal particles and mechanical behavior of soft gels with the primary objectives of (a) determining the

processes by which different effective interactions contribute to the mechanical properties, (b) providing a link between macroscopic stress and microstructural changes taking place during deformation, and (c) identifying universal interaction-independent mechanical properties, if any. To this end, we use a short-range effective interaction for modeling the mechanical behavior of gels. We first discuss the methodology used to assemble gel networks and detail the numerical investigation carried out to obtain their mechanical behavior. Afterwards, microstructural properties of the gels and their mechanical response to shear deformation are studied. In particular, the homogenized stress–strain response and local geometric properties of the gels are of interest. Analytical study of the potentials is conducted in order to discuss the mechanical behavior of gels in terms of the mathematical formulation of their effective interactions. Furthermore, the findings are compared with those from two other existing gel models, using repulsive many-body interactions, in order to better assess the influence of the potential selection.

Computer models and numerical simulations

The microstructural properties and mechanical behavior of soft gels are investigated by a numerical particle gel model in which particles can self-assemble into random network structures [23]. Among different models used for this purpose [29], this work assumes that gel networks can be generated from a set of N particles of diameter d and mass m interacting through a potential Ψ with 2-body and 3-body terms ψ_2 and ψ_3:

$$\Psi = \varepsilon \sum A\psi_2\left(\mathbf{r}\right) + B\psi_3\left(\mathbf{r}, \mathbf{r}'\right). \quad (1)$$

In the above equation, constants A and B control the relative intensity of the 2-body and 3-body terms. The 2-body term ψ_2 is responsible for the attractive interactions between particles and is a function of the bond vector $\mathbf{r}$ of length $r = |\mathbf{r}|$, figure 1(a). The 3-body term ψ_3 maintains the open network structure by means of repulsive interactions.

At a given volume fraction ϕ and temperature T, the onset of gelation depends on the attraction intensity, or energy scale ε, as well as the range of the attractive potential [15]. The energy scale ε determines the phase behavior of the systems. For a given thermal energy k_BT, the choice of ε/k_BT

controls the gelation process: at high temperatures, we obtain a colloidal suspension with particles in a gas phase, at low temperatures, we obtain a gel made up of connected chains of particles. The range of interaction potentials has consequences on the topology and possibly mechanical properties of the gels: short-range interactions generate short chains of particles that can resist bending, and long-range interactions generate longer chains whose stability is provided by interactions with other chains [16].

For real systems, the precise expression of the interparticle interactions is rarely known. Here, a generalized Lennard-Jones potential is selected for the 2-body term ψ_2 in equation (1) [10, 21, 23]. The width of the well of this centrosymmetric potential determines whether interactions between particles are short-ranged (narrow well) or long-ranged (wide well). Because particles interacting with each other only through a centrosymmetric 2-body potential aggregate into a single solid phase, a 3-body term is required for enforcing the particles to form an open fractal geometry. This 3-body term must be repulsive in order to generate open gel networks whose microstructure resembles what has been observed experimentally [18, 33].

The 2-body and 3-body terms are assumed to have the following general forms:

$$\psi_2\left(\mathbf{r}\right) = \Lambda_2\left(r\right) f_2\left(r\right) \tag{2a}$$

$$\psi_3\left(\mathbf{r}, \mathbf{r}'\right) = \Lambda_3\left(r\right) \Lambda_3\left(r'\right) f_3\left(\theta\right) \tag{2b}$$

where $\theta = \mathrm{acos}(\mathbf{r} \cdot \mathbf{r}'/r\, r')$ is the angle between two bond vectors $\mathbf{r} = \mathbf{r}^{ij}$ and $\mathbf{r}' = \mathbf{r}^{ik}$ departing from a particle, figure 1(a), r and r' are bond vector lengths, Λ_2 and f_2 are 2-body modulation and potential function, respectively, and Λ_3 and f_3 are 3-body modulation and potential function, respectively. The radial modulation terms ensure continuity of interaction potentials; they are zero at the cutoff distance and increase as the interparticle distance approaches the particle diameter in the present work. Thus, only particles that are close enough to one another could interact with each other. The choice of potential terms ψ_2 and ψ_3 determines the exact form of the network microstructure. For instance, 3-body terms that are repulsive for all values of bond angles favor straight chains [27]. Furthermore, 3-body terms which are only repulsive for low bond angles allow multiple equilibrium configurations with large bond angles [28]. The latter may result in systems with multiple equilibria and with zero-energy deformation modes.

Here, we consider the following potential for the interaction between particles,

$$f_2\left(r\right) = \frac{b}{r^{18}} - \frac{1}{r^{16}}, \qquad \Lambda_2\left(r\right) = e^{\frac{1}{r-a}} \tag{3a}$$

$$f_3\left(\theta\right) = \left(\cos\theta + \alpha\right)^2, \qquad \Lambda_3\left(r\right) = e^{\frac{\Gamma}{r-a}}. \tag{3b}$$

The above equations are obtained from modifying the Stillinger-Weber potential, which was initially developed to model crystalline silicon and has been successfully modified for modeling other media such as amorphous silicon, glasses, quasi-brittle materials and long-range colloidal gels

[27, 34–38]. By selecting the parameters of the 2-body term (3a) and 3-body term (3b) as $A = 29.215$, $b = 0.896$, $a = 1.9$, $B = 40$, $\alpha = 1$ and $\Gamma = 2$, we obtain a particle gel model capable of producing gels with desired properties such as stable short chains with bending resistance, preferred straight configuration, and no zero-energy deformation modes. In the sequel, 'potential', 'model' and 'effective interactions' are used interchangeably. Furthermore, the length, mass and energy values are reported in reduced units of d, m, and ε, respectively.

For comparison purposes, the numerical results from two other forms of interaction potentials are also considered. The particle gel model based on the short-range effective interaction with a Gaussian 3-body term, referred to here as the SRG model, has been successful in capturing different aspects of the mechanical behavior of colloidal gels [28, 31, 32, 39, 40]. The 2-body term of the SRG model is given by the short-range attractive interaction and without any radial modulation, i.e.

$$f_2^{\mathrm{SRG}}\left(r\right) = \frac{b}{r^{18}} - \frac{1}{r^{16}}, \qquad \Lambda_2^{\mathrm{SRG}}\left(r\right) = 1 \tag{4a}$$

and the 3-body potential term is given by

$$f_3^{\mathrm{SRG}}\left(\theta\right) = \exp\left(-\frac{\left(\cos\theta - \cos\theta_0\right)^2}{w^2}\right),$$
$$\Lambda_3^{\mathrm{SRG}}\left(r\right) = \frac{1}{r^{10}}\left(1 - \left(\frac{r}{2}\right)^{10}\right)^2. \tag{4b}$$

The effective interaction is defined by choosing $A = 6.27$, $a = 0.85$, $B = 67.27$, $\theta_0 = 65°$ and $w = 0.3$. This set of parameters is one convenient choice (among yet unexplored other choices) that facilitates self-assembly of particles under isothermal conditions.

Furthermore, the modified Strillinger-Weber potential, referred to here as the MSW model, is based on the Stillinger–Weber potential, which was initially developed to model crystalline silicon [27, 34]. Different versions of this potential have been used to model the behavior of gels, amorphous silicon, glasses, and quasi-brittle materials [27, 35–38]. The 2-body and 3-body potential functions of the MSW model are given by

$$f_2^{\mathrm{MSW}}\left(r\right) = \frac{b}{r^4} - 1, \qquad \Lambda_2^{\mathrm{MSW}}\left(r\right) = e^{\frac{1}{r-a}} \tag{5a}$$

$$f_3^{\mathrm{MSW}}\left(\theta\right) = \left(\cos\theta + \alpha\right)^2, \qquad \Lambda_3^{\mathrm{MSW}}\left(r\right) = e^{\frac{\Gamma}{r-a}}. \tag{5b}$$

The models parameters are chosen as $A = 7.0496$, $b = 0.6022$, $a = 1.8$, $B = 10$, $\alpha = 1.49$, $\Gamma = 1.2$. Similarly as the SRG model, this set of parameters is one possible choice that generates networks composed of many interconnected particle chains [38].

Gelation protocol

The numerical gel networks are obtained from colloidal particles using the following procedure [23]. Starting from a gas phase of randomly placed particles in a box, we bring the system to a temperature $\varepsilon/k_{\mathrm{B}}T = 20$ using the Nosé–Hoover

thermostat over 5×10^6 time steps. As the temperature is decreased, the particles gradually aggregate into clusters until they form arrested networks spanning the entire simulation box. The networks obtained at that temperature are persistent because the thermal energy $k_B T$ is small enough compared to the energy scale of the interactions ε, i.e. thermal fluctuations cannot break the bonds formed between the particles. The systems are equilibrated by a thermostatted run at the final temperature for another 5×10^6 time steps. In order to solely identify the role of the enthalpic potential and to cancel out the effects of thermal fluctuations, we subsequently quench the system using the damped dynamics, i.e.

$$m\ddot{\mathbf{x}} + \xi\dot{\mathbf{x}} + \nabla\Psi = 0 \qquad (6)$$

until the thermal energy becomes negligible compared to the potential energy [28]. The value of the damping parameter is taken as $m/\xi = 1.0$ τ and the characteristic time $\tau = (md^2/\varepsilon)^{1/2}$ is defined by the scales of energy ε, length d, and mass m [31]. The above protocol is used to generate networks from $N = 50\,000$ particles in cubic periodic boxes of size $L = 80.60d$, $63.97d$ and $55.88d$, corresponding to volume fractions $f = 0.05$, 0.10, 0.15, respectively, figure 1(b). All numerical simulations have been done using the LAMMPS Molecular Dynamics software [41].

Mechanical characterization

The mechanical response of the particle gel model stems from the same effective interaction Ψ responsible for the self-assembly of colloidal particles into a network structure. We investigate the athermal nonlinear mechanical response of particle gel models under strain-controlled volume-preserving simple shear deformation. For a given strain level γ, the shear kinematics is characterized by:

$$\mathbf{x}^i = \mathbf{\Gamma}\mathbf{X}^i, \quad \mathbf{\Gamma} = \Gamma_{mn}\mathbf{e}_m\mathbf{e}_n, \quad m, n = 1, 2, 3 \quad \text{and } i = 1 \ldots N \qquad (7)$$

where $\mathbf{x}^i$ and $\mathbf{X}^i$ are the respective position vectors of the ith particle after and before deformation. $\Gamma_{11} = \Gamma_{22} = \Gamma_{33} = 1$, and $\Gamma_{12} = \gamma$ are the nonzero components of $\mathbf{\Gamma}$. Strain deformation is applied in finite steps $d\gamma = 0.01$ until yielding occurs. At each step, all particles are first deformed affinely. Following this affine shear step, the system will be out of equilibrium. Thus, the position of particles should be relaxed to reach equilibrium in the deformed configuration. To assess the sole contribution of the potential and the topology of gel networks, disregarding viscous effects introduced by (6), relaxation is performed using athermal quasistatic shear (AQS) [42, 43]. This methodology determines the relaxed configuration of the system by solving $\nabla\Psi = 0$ using the classical energy minimization techniques, instead of solving (6) by finite shear rate simulations [39]. It is noted that both finite shear rate and AQS techniques are equivalent in the limit of very low shear rate ($\ddot{\mathbf{x}} \sim 0$ and $\dot{\mathbf{x}} \sim 0$).

We study the homogenized stress–strain response of the gels when they are subjected to shear deformation. The homogenized shear stress is given by the virial stress [44], i.e. the shear stress at each increment is obtained from

$$\sigma_{12} = \frac{1}{V}\sum_{i,j}\frac{\partial\Psi}{\partial r_1^{ij}}r_2^{ij} \qquad (8)$$

where V denotes the volume of simulation box, and σ_{12} is the shear stress corresponding to the applied shear strain. The formula (8) might cause slight errors in stress estimates near the boundaries of the simulation box. The differential modulus $K = \partial\sigma_{12}/\partial\gamma$ is calculated from the stress–strain response at each strain increment; the initial differential modulus is referred to as G. We investigate the microscopic rearrangements of the gel network topology during various phases of the deformation in order to provide a quantified space-resolved microscopic explanation for their nonlinear mechanical response. Results obtained for the particle gel model of the present study are compared with those from other well-documented gel models, belonging to the general class of potentials (2), in order to assess the influence of the potential selection on the response of particle gel models. Specifically, we consider the short-range effective interactions with a Gaussian 3-body term, and the modified Stillinger–Weber potential [27, 28, 34, 38]. The SRG model produces spanning networks made up of chains of particles, joint at nodes with coordination 3 and has successfully provided numerical insight into key aspects of gel behavior such as the microscopic origins of non-local processes, the self-assembly dynamics, the mechanical behavior and its link with network topology as well as aging [18, 28, 31–33, 39, 44]. All data reported for the SRG model in the present work have been obtained from the literature [28, 31, 39, 40]. The MSW model, differs from the SRG model in its formulation; yet, it similarly produces spanning networks of chains connected at nodes with coordination 3 and could be used to investigate the equilibrium dynamics of gels. Since the data required for comparing the results of the present work with those of the MSW model are unavailable in the literature, numerical simulations using the MSW model are also performed here.

Results and discussion

Homogenized response to shear deformation

The variation of the homogenized shear stress component σ with the applied shear strain is schematically depicted in figure 2(a). The numerical stress–strain response is in agreement with experimental data for colloidal and polymer gels under direct shear [9, 45, 46]. The nonlinear response presents four different phases. At small strain, the systems are very soft with an initial shear modulus G. In this first region, particle gel models often exhibit slight softening where the differential modulus $K = \partial\sigma_{12}/\partial\gamma$, corresponding to the slope of the stress–strain curve, decreases with increasing the strain. The softening continues up to the strain γ_1 (and the corresponding stress σ_1) where K reaches a local minimum. It is noted that some systems may not exhibit the initial softening and show a purely linear initial response with a constant differential modulus up to the strain γ_1 (represented by the dashed line in figure 2(a)). Afterwards, the second phase of the response
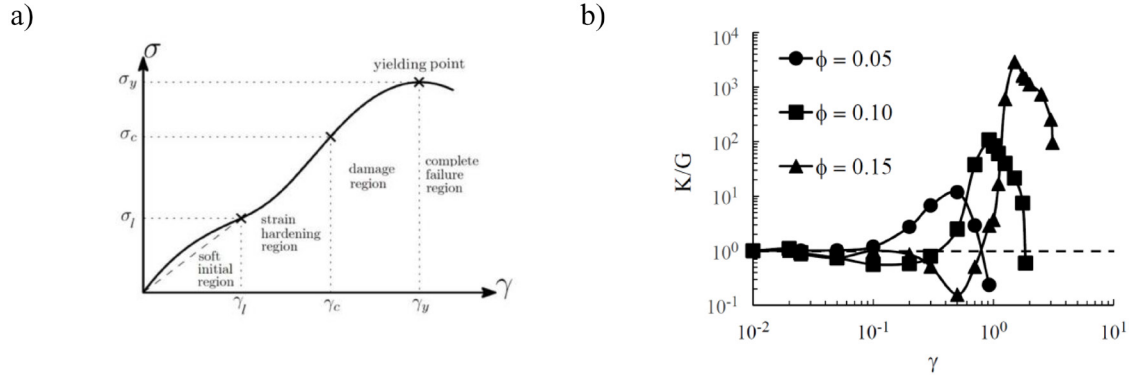
a)

b)

Figure 2. (a) Schematics of the stress–strain response along with all different phases of the deformation. The dashed line represents the case of an initially linear response. (b) Variation of the normalized differential modulus *K/G* against the applied shear strain for the present model at three different volume fractions.

begins and strong strain hardening is observed. The differential modulus can span multiple orders of magnitude as observed in biopolymer gels [45].It is known that the non-affine bending of the filaments affects the hardening behavior of semiflexible fiber networks [47–49]. However, the non-affinity is expected to promote strain softening response in particle-based models [42, 50]. The systems reach their maximum stiffness at the critical strain γ_c (and the corresponding critical stress σ_c). Then, the response enters the damage region, which corresponds to the development of irreversible mechanisms and damage accumulation because of local breaking of interparticle bonds. The stiffness of the systems decreases until it vanishes. The maximum stress occurs at the yield strain γ_y, after which systems enter the complete failure region and undergo shear flow [51]. The normalized differential modulus *K/G* is plotted against the strain for the present model in order to show the effect of volume fraction on the mechanical response (figure 2(b)). We can easily determine the nature of the initial response and identify the different phases of the deformation. The proposed model shows strain-softening at low volume fractions ($\phi = 0.05$ and $\phi = 0.10$) with a decrease of the normalized differential modulus to values lower than 1. The minimum differential modulus is smaller at the lowest volume fraction. At $\phi = 0.15$, the curve is initially horizontal, indicating a constant differential modulus and a purely linear response at small strain. The strain γ_l decreases with increasing volume fraction and the shift to the strain-hardening phase occurs at smaller deformation. The critical strain and the maximum value of differential modulus during the strain hardening phase decrease with increasing volume fraction. These observations indicate that microstructural reorganizations are more important at low volume fractions where gel networks are more fibrillar and composed of loosely connected chains.

The softening at low volume fractions and the brittle response of gels at high volume fractions have also been reported for particle gel models constructed using the SRG model [31]. Thus, the results obtained with the present model indicate that different potentials can lead to comparable mechanical responses, offering new possibilities of potential
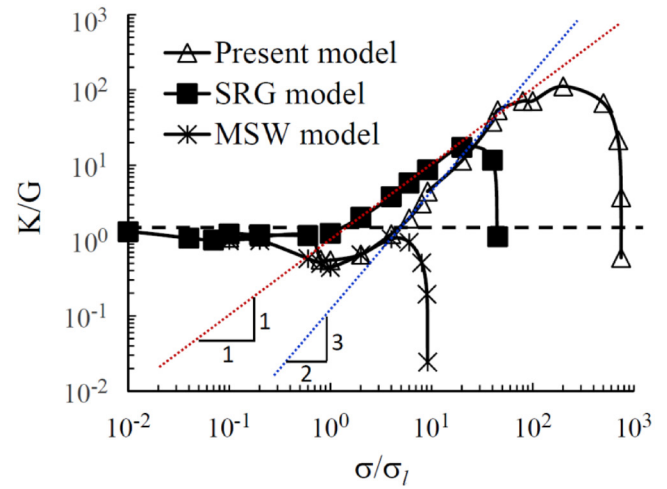

Figure 3. Comparison of the normalized differential modulus versus normalized stress for different gel models at $\phi = 0.10$. The dashed lines show that the differential modulus scales as power-law with exponents of 1 and 1.5 for the present and SRG models, respectively.

selection for modeling of the mechanical response of soft gels. Figure 3 compares the normalized differential modulus *K/G* for the SRG and MSW models at $\phi = 0.10$ to that of the present model, figure 3. As described previously, the present model shows initial strain-softening followed by a significant increase in *K* of several orders of magnitude. The differential modulus scales as power-law with the stress $K \sim \sigma^{\nu \geqslant 1}$ over the strain hardening-phase, a typical behavior of semiflexible fiber networks [47, 52–54]. The SRG model also shows an almost initial linear response followed by a strain-hardening region, but the scaling has a smaller exponent $\nu \sim 1$ compared to $\nu \sim 1.5$ of the present model. On the other hand, the MSW Model shows very little hardening ($\nu = 1$) following the initial softening region and barely reaches the value of the initial shear modulus even at very large shear strains. These differences in the behavior of particle gel models generated with different potentials indicate that the volume fraction alone cannot fully determine their mechanical response and different responses could be obtained using distinct potential formulations.
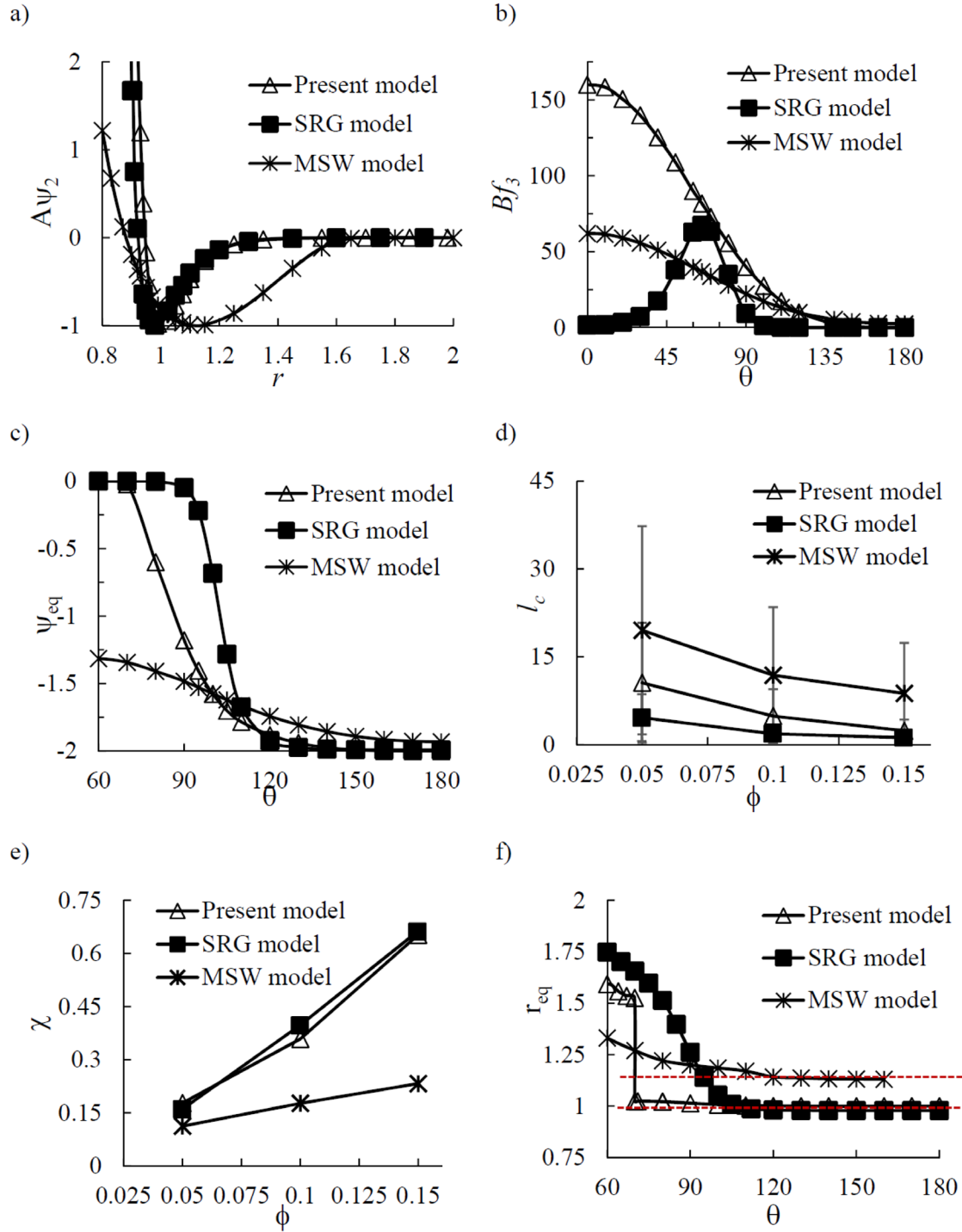
Figure 4. Comparison of the effective interactions of the present model, SRG model, and MSW model: (a) 2-body term A ψ_2; (b) 3-body potential function Bf_3; (c) potential Ψ for 3-particle system, flat regions indicate equilibrium configurations. Comparison of topology of gel models, i.e. (d) mean chain length l_c, (e) proportion of bonds c participating in nodes of coordination 3. (f) bond equilibrium length r_{eq} as a function of the bond angle. The increase of r_{eq} at low angles is possibly because of the repulsive effect of the 3-body term.

Interaction potential properties and gel topology

The physical origins of the homogenized response of particle gel models can be determined by analyzing their mathematical formulation and specific properties of their interaction potentials. The 2-body term A ψ_2 is plotted as a function of the bond length r in figure 4(a). The present model is clearly a short-range one because of the narrow width of its potential

well, i.e. local particle interactions dominate the mechanical behavior of the particle gel model. The 3-body term Bf_3 is plotted as a function of the bond angle θ in figure 4(b). The present model has a repulsive 3-body term with the preferred equilibrium value $\alpha = 1$, i.e. a stable equilibrium exists for straight chains ($\theta = 180°$). Studying the equilibrium response of the 3-particle system shown in figure 1(a) will provide additional insight into the possible equilibrium configuration

of particle assemblies. For various values of the bond angle θ, we find the equilibrium configuration of the 3-particle system by minimizing the potential Ψ, which is equal to the sum of all 2-body, i.e. (i–j, j–k, k–i), and 3-body interaction terms, i.e. (i–j/k, j–i/k, k–i/j), between the three neighboring particles. The potential at equilibrium is plotted for all values of θ in figure 4(c). At small angles where the 3-body modulation is zero, the potential Ψ vanishes for the model proposed in the present study. Furthermore, a stable equilibrium state exists at $\theta = 180°$ where the bonds are perfectly aligned. Next, the effects of the present potential formulation on the gel topological parameters are discussed. Figure 4(d) confirms that the mean length l_c of the chains between two nodes of coordination 3 is rather short and decreases with the volume fraction. The proportion of interparticle bonds attached to the network nodes of coordination 3, denoted by χ [31], is strongly dependent on the gel volume fraction ϕ, figure 4(e). At low volume fractions, the gel networks are loose and fibrillar with longer chains while at higher volume fractions, they are composed of densely connected short chains. Figure 4(f) shows that the equilibrium length of the bonds $r_{eq}(\theta)$ in the gels created by the present model depends on the bond angle. Should the bond length only depend on the 2-body term, the equilibrium length would be independent of the bond angle and equal to the length that minimizes the 2-body term (dashed lines in figure 4(f)). For the present model, the equilibrium length is almost equal to 2-body equilibrium length and shows little variations for large bond angles $\theta > 110°$.

Next, the features of other particle gel models are discussed in comparison with the present model. Because of the wide potential well of the MSW model, remote interactions between particles will influence the behavior of gel models constructed using this long-range model. The SRG Model has a nearly identical 2-body term as the proposed model in this work (figure 4(a)); yet gels with different topology and mechanical response are obtained. Therefore, the short-range 2-body term does not fully characterize the behavior of these gel networks and the 3-body term plays a strong role. In particular, the repulsive Gaussian form of the 3-body term in the SRG model makes small angles unlikely. For the MSW model, the equilibrium angle, corresponding to the 3-body term, is not chosen by the systems; thus, a repulsive branch without stable equilibrium exists, figure 4(b). It is interesting to note that all models have a configurational equilibrium for the angle $\theta = 60°$ where particles arrange themselves into a self-stable self-stressed equilateral triangle, figure 4(c). The SRG Model shows two flat regions, $\theta < 80°$ and $\theta > 140°$, with constant and vanishing potential. Because the potential is constant for a number of different configurations, there exists multiple equilibria which may explain reported difficulties to perform energy minimization for the particle gel models created by the SRG model [31]. For the long-range MSW model, the potential continuously decreases with increasing the bond angle and never reaches a stable equilibrium. Thus, the most favorable region of the equilibrium should be reached at large angles, where the potential variations are smaller. Because the potential has no stable minimum, the stability and equilibrium

of the gel model is more likely to be conferred by the interactions with other particles; this statement agrees with previous numerical results and experimental observations [16]. In terms of the network geometry, the SRG model and MSW model, respectively, have shorter and longer chains than the present model. The length distribution is similar for all models with the standard deviation nearly equal to the mean chain length, regardless of the volume fraction, figure 4(d). The bond proportion χ is nearly identical for short-range models and much larger than that of the long-range MSW model. The latter maintains a fibrillar topology, with long chains and few nodes, even at moderate volume fractions, figure 4(e). The differences in chain length l_c for identical node density χ for the present model and SRG model indicate differences in the connectivity of the networks resulting from clear differences between 3-body terms. Similar to the present model, the equilibrium bond length r_{eq} is constant at large angles ($\theta > 110°$) for the short-range SRG model and the value of the equilibrium length is equal to the 2-body equilibrium length, figure 4(f). The bond angle distribution for the SRG model indicates that networks assemble with angles larger than 110°. For the long-range MSW model, the equilibrium distance decreases but remains larger than that of the corresponding 2-body term, even for the aligned bonds ($\theta = 180°$). This observation indicates that the 3-body term i–j/k generates repulsive forces in the direction of the bonds, which is a consequence of the radial modulation term Λ_3 in the 3-body interaction potential. Indeed, taking the derivative of (2b) with respect to one bond vector r results in a repulsive force in the direction of that bond vector for large values of the potential function $f_3(\theta)$ and the derivative of the modulation $\partial \Lambda_3 / \partial r$. The axial interplay between the 2-body and 3-body terms has two major consequences on the mechanical response of gel networks generated by the MSW model. First, because of the axial contribution of the 3-body term, it is not possible to independently assign the 2-body and 3-body terms to the stretching and bending processes, respectively. For the MSW model, the 3-body term varies when the particle bonds are stretched at a constant bond angle. Second, because the equilibrium bond length decreases with increasing the bond angle, chains of multiple bonds at equilibrium have shorter contour lengths when they are straight than when they are curved. As discussed in the following section, this latter observation could have important consequences on the mechanical behavior and evolution of the network microstructure during deformation.

Mechanical stress breakdown

The nature of local processes is highlighted by separating the stress into contributions from the 2-body and 3-body terms. Because of the evolution of the gel microstructure under large strains, different physical phenomena are expected to dominate their mechanical response at different phases of the deformation. Here, we study the homogenized shear stress breakdown for low ($\phi = 0.05$) and moderate ($\phi = 0.15$) volume fraction gels in order to highlight the influence of the volume fractions, figure 5. For the gels created using the
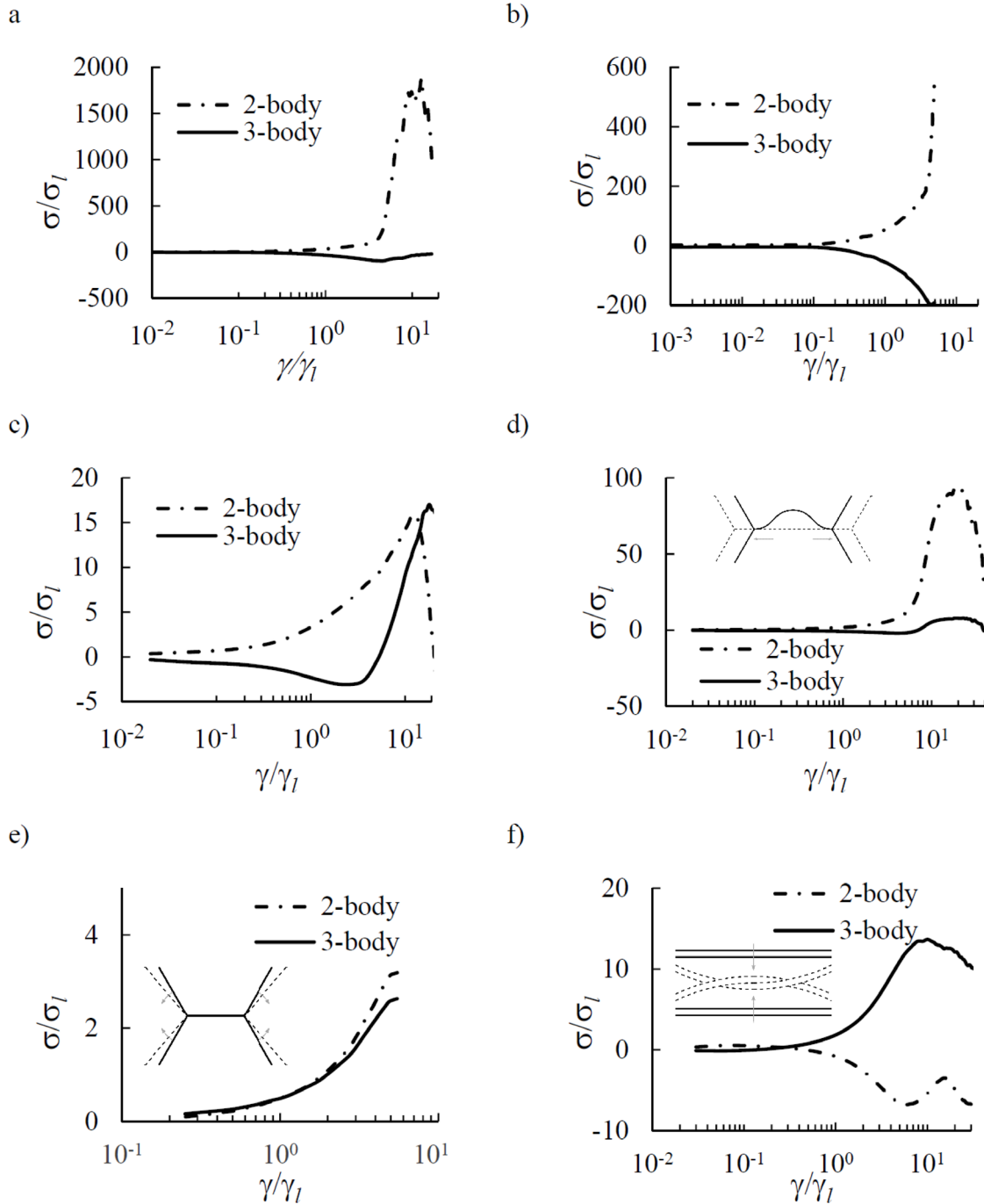
Figure 5. 2-body and 3-body stress breakdown for all models at low volume fraction $\phi = 0.05$ using (a) present model, (b) SRG model, (c) MSW model, and moderate volume fraction $\phi = 0.15$ using (d) present model, (e) SRG model, (f) MSW model. Stress is mostly borne by stretching while the initial release of residual bending stress makes the 3-body stress contribution negative. The different response of MSW model indicates that the behavior of these systems is mainly dominated by volume exclusion constraint and contact between chains, rather than bending and stretching of chains. The insets show pictorially how the particle chains resist the external deformation.

potential functions proposed in this work (figures 5(a) and (d)), the bonds primarily resist deformation by stretching, i.e. the 2-body potential term contributes the most to the stress response. Interestingly, the 3-body term initially favors the deformation with negative contribution to the stress. This negative contribution is observed because curly chains uncoil into a straight configuration, thereby releasing their residual stress. The 3-body term, especially in gels with high volume fractions, will have a positive contribution to the load-bearing

capacity of the gels when the applied shear strain becomes large. Similar mechanical stress breakdown is seen for the SRG model at low volume fraction, figure 5(b). For that model, the 2-body and 3-body terms equally contribute to the stress response at moderate volume fraction, figure 5(e). The origin of the 3-body contribution to the homogenized shear stress of these particle gel models can be explained in terms of their denser topology compared to that of the networks generated using the MSW model, figure 4(d). Short chains are

straighter and bend around nodes; thus, the 2-body term and 3-body component of the potential resist the applied deformation by stretching and bending of the chains, respectively. The response of networks created by the MSW model greatly differs from that of the short-range models; this is expected because of clear differences in the geometry of these gels. At low volume fractions (figure 5(c)), the stress breakdown resembles that of the other models at low strain. However, significantly different response is seen during the non-linear phase of the deformation, which is because the 3-body interaction term strongly resists the deformation. In other words, both 2-body and 3-body terms participate equally in the stress response up to the maximum stress. At the beginning of the damage region, breakage of bonds releases the axial stress and the 2-body term favors while 3-body term resists deformation. As the volume fraction is increased (figure 5(f)), we observe a different response where the 2-body term favors the deformation while the 3-body term resists it. Such behavior, especially the negative contribution of the 2-body term, cannot solely be explained by stretching and bending mechanisms. These results suggest that the fibrillar topology of the MSW model at larger volume fraction causes the response to be dominated by the excluded volume constraint and remote interactions between fully formed chains of particles. As two chains approach one another, they are pulled together by the long-range 2-body term and strongly repelled by the 3-body axial repulsion. Such mechanism does not occur for the model proposed in the present study since the interactions have shorter range. Moreover, the present particle network models are more densely connected and less fibrillar; thus, the contact between fully formed chains is less likely to occur.

Particle network models show negative normal stress and all components of the stress tensor are expected to participate in resisting the applied deformation [55]. This phenomenon can be further investigated by analyzing the evolution of principal homogenized stresses. The eigenvectors of the stress tensor σ give the principal directions of stress $\mathbf{v}_I$, $\mathbf{v}_{II}$, $\mathbf{v}_{III}$ and the corresponding eigenvalues give the principal stress values σ_I, σ_{II}, σ_{III}. For the proposed model (figure 6), the stress is mostly borne by tensile stress σ_I in the principal direction $\mathbf{v}_I$, nearly overlapping with the direction $(1,1,0)$ of the simulation box. The principal stress σ_{II} in the transverse direction $\mathbf{v}_{II}$ and σ_{III} in the out-of-plane direction $\mathbf{v}_{III}$ are small compared to σ_I. The breakdown of principal stresses between 2-body and 3-body is shown in the figure 6(b). We can observe that there exists a competition between the 2-body and 3-body terms. Most of the 2-body principal stress is in the $\mathbf{v}_I$ direction. In the other directions, the 3-body term, with an opposite sign but almost equal value to the 2-body term, results in low principal stresses σ_{II} and σ_{III}. The networks created by the MSW model (figure 7(a)) show a similar response with large principal tensile stress σ_I in the $\mathbf{v}_I$ direction and small stress in other directions. The breakdown into 2-body and 3-body principal stress; however, differs significantly, figure 7(b). We observe very large values of both 2-body and 3-body principal stresses in every direction, even in the directions $\mathbf{v}_{II}$ and $\mathbf{v}_{III}$, where the total stress is small. These values can be twice as large as the total maximum principal stress and point to the strong

competition between the 2-body and 3-body terms. The above discussion further explains the stress breakdown shown in figure 5 and highlights the importance of 2-body and 3-body interactions between colloidal particles in load-bearing properties of colloidal gels; these interactions cannot be simply mapped to stretching and bending processes especially for long-range models.

### Physical origins of the initial softening

Strain softening has been observed experimentally and numerically in soft colloidal gels of different nature and under various loading conditions [31, 56, 57]. This behavior is believed to arise from the complex interplays of entropic and enthalpic contributions in the systems whose topology is primarily fibrillar such as polymer and colloidal gels [16, 27, 28, 58]. Most experimental work addressing the stiffness of gels focuses on rheology tests, i.e. the use of oscillatory shear experiments [56, 57, 59]. Numerical models have demonstrated strain softening of low volume fraction colloidal gels under direct shear using finite shear rate simulations with viscous effects [31]. However, this approach cannot fully separate the entropic and enthalpic contributions, and subsequently could only provide an overall picture of the initial strain softening behavior of gels. Here, AQS simulations are performed on particle gel models in order to account for the sole enthalpic contribution in their strain softening behavior. This approach allows us to study the mechanical behavior resulting only from the gel network topology and the interparticle interactions, canceling out possible effects of the viscosity and thermal fluctuations. The stress–strain behavior in the initial phase, i.e. when the strain is lower than the strain γ_l, is a consequence of the stress breakdown. In other words, 2-body and 3-body processes compete with each other and the rate at which each process increases with the strain determines the softening behavior of the gels. Because colloidal particles form connected chains, the topology of gel models resembles that of fiber network models, which are widely used to investigate the mechanical behavior of polymer networks [52, 60]. For such systems, it has been observed that geometric reorganization, such as rotation and stretching of the fibers, influences their nonlinear mechanical response [47, 48, 61, 62].

In this section, we investigate how individual bonds participate in the overall mechanical response of particle gel models. It is seen that the stress becomes concentrated in selected bonds oriented in their bond vector direction $\hat{\mathbf{r}} = \mathbf{r}/r$. We define the following measure,

$$\Theta = |\mathbf{r} \cdot \mathbf{v}_I| \tag{9}$$

which characterizes the alignment of bonds in the direction $\mathbf{v}_I$ of the maximum principal stress σ_I. We evaluate the Pearson correlation coefficient (PCC) between the bond alignment Θ and the bond stretch r/d for all interparticle bonds in the system, figure 8. Initially, the systems are unstrained and isotropic; thus, no correlation between stretch and alignment exists. As the strain is increased, microstructural reorganizations occur and we observe an initial decrease of the PCC to negative values, i.e. the stretch in fibers and their alignment
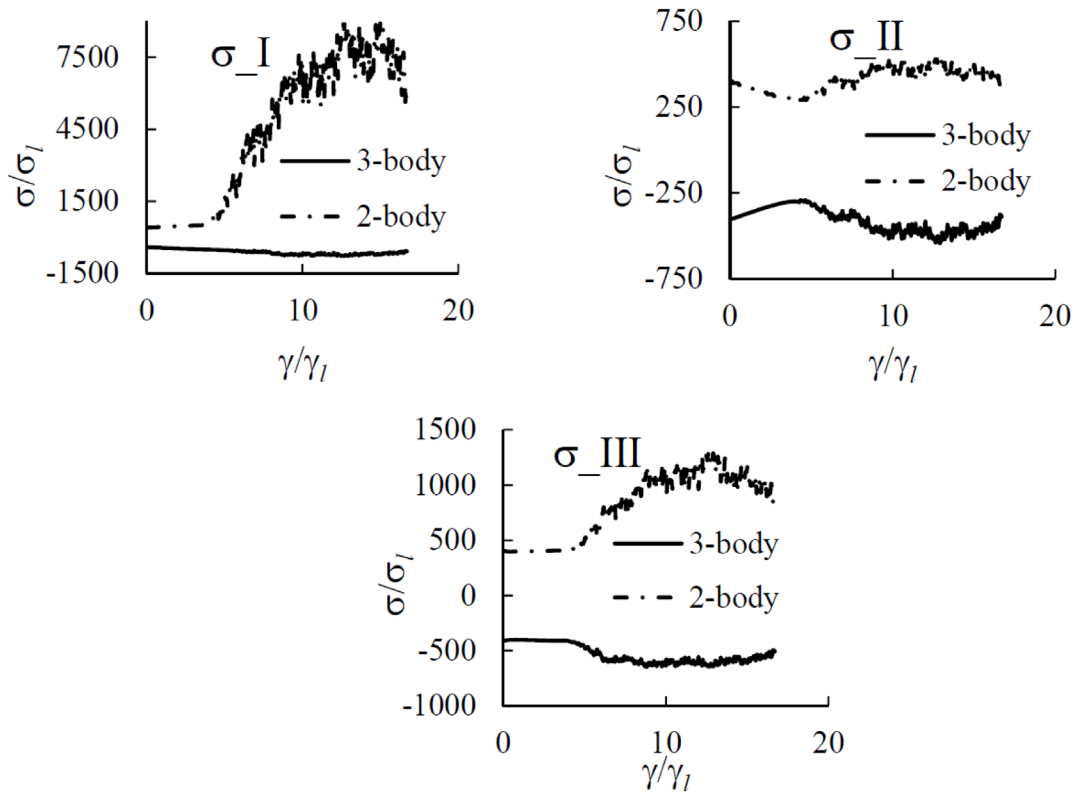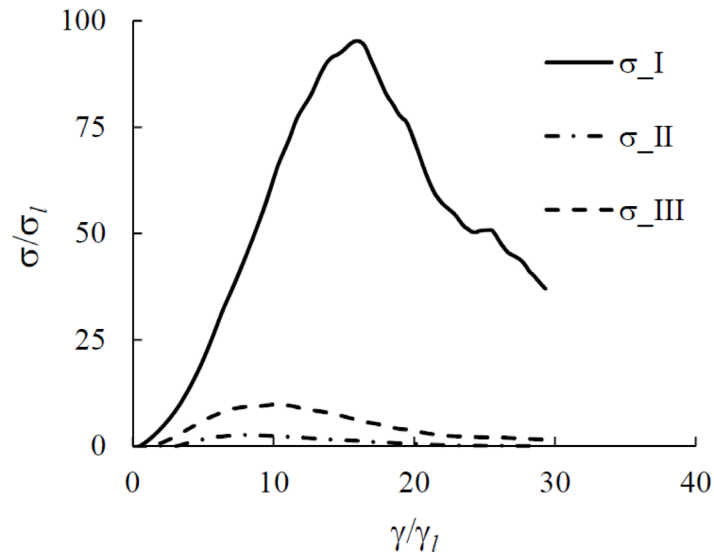
a)
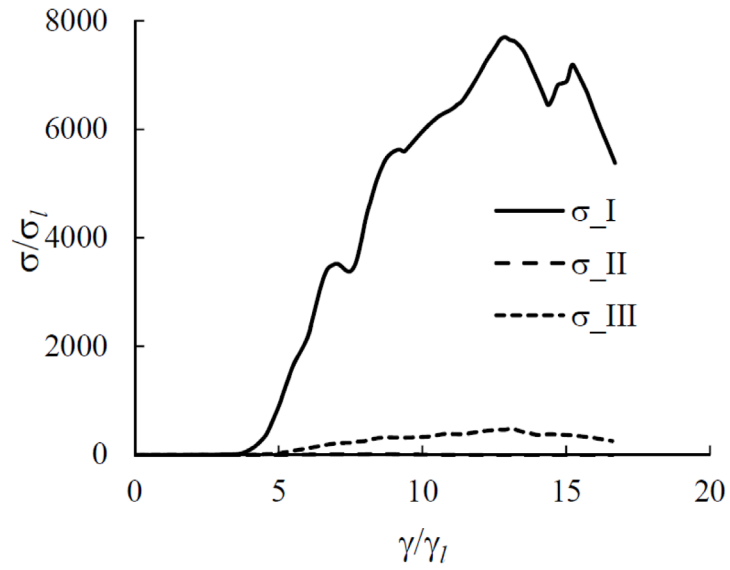
b)

Figure 6. (a) Normalized principal stresses as a function of normalized shear for the present model at $\phi = 0.05$. (b) The 2-body and 3-body breakdown in each principal direction.

in the principal stress direction have an anticorrelation. This anticorrelation provides additional explanation for the origin of the initial softening phase of the stress–strain response that is observed in figure 2. In particular, it can be noticed that networks exhibiting the most softening (figure 2(b)) also have the largest anticorrelation, figure 8. In literature [31], this shear softening has been attributed to the disturbance of the initial

self-stressed arrangement of curly chains whose equilibrium configuration is straight, i.e. the initial 3-body bending energy of curly chains is released during the deformation and as they become straight. This argument is supported by the observation that polymer networks with comparable topologies, but without residual bending stress, do not show the initial shear softening response [52, 63]. The findings of the present study;
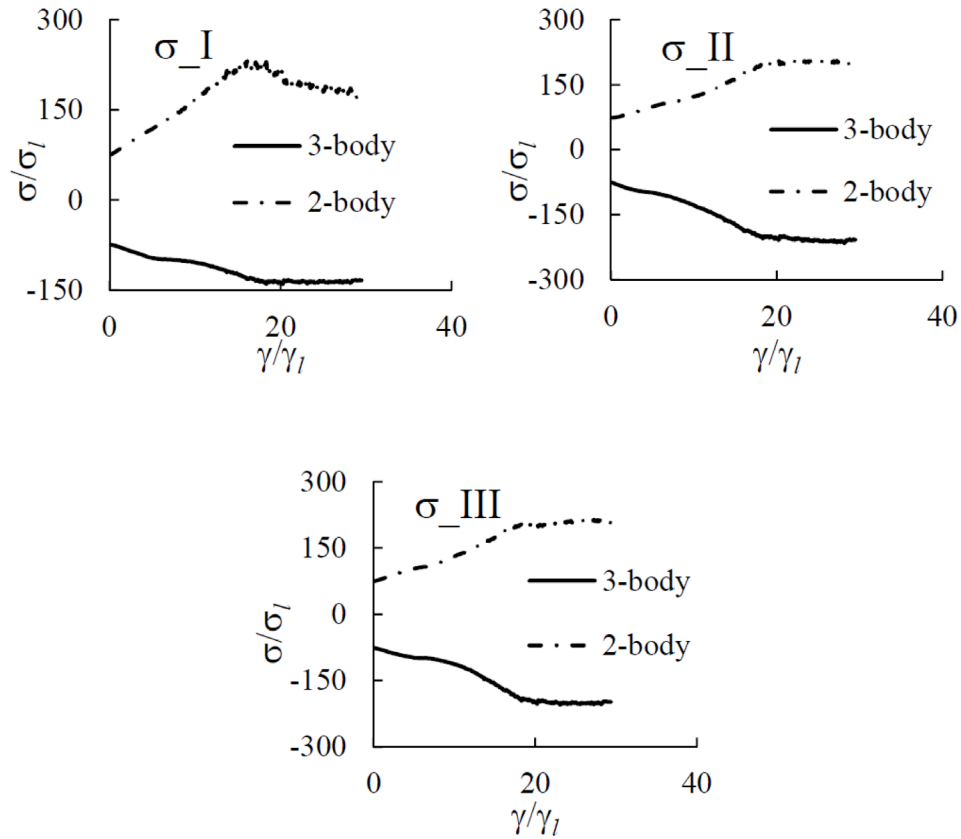
a)

b)

Figure 7. (a) Normalized principal stresses as a function of normalized shear for the MSW model at $\phi = 0.05$. (b) The 2-body and 3-body breakdown in each principal direction.

however, suggest that the bond stretch, associated with local 2-body stresses, could be another important mechanism. In other words, in addition to the release of 3-body bending stress because of chain uncoiling, the initial rearrangement of the chains redirects their 2-body stretching stress away from the direction of global principal stress. Following the initial decrease, the correlation increases to positive values and reaches a maximum value at strain levels around the critical strain. During this phase, straightened out fibers elongate as a result of the applied deformation and the correlation is positive for all models. In the damage region, the correlation stabilizes or decreases again as strong topological reorganizations
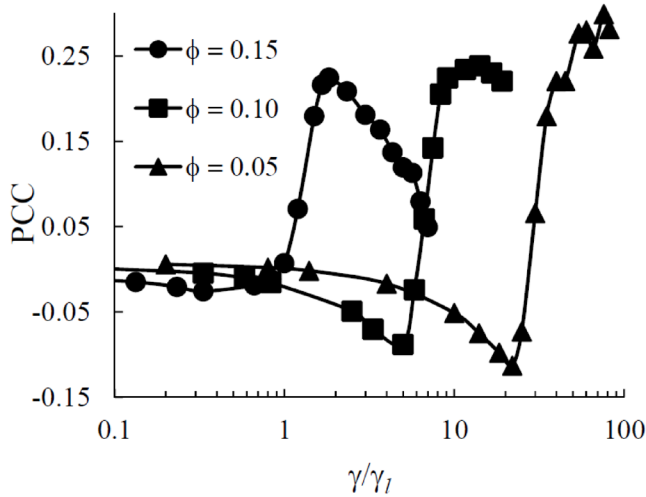
Figure 8. PCC between the alignment Θ and the stretch for all interparticle bonds in the present model at different volume fractions.

occur because of breaking and forming new interparticle bonds. Bonds aligned in the direction of principal stress carry less stress, explaining the decrease of stress during the final shear flow, i.e. complete failure region, figure 2(a). The above discussion suggests that non-affine displacements play a significant role in the observed nonlinear stress–strain behavior and could be used to provide a better microscopic interpretation of the mechanical response of particle gel models [64, 65]. However, such studies are beyond the scope of the present work.

Conclusion

The present paper investigated the influence of the effective interaction potential between colloidal particles on the mechanical behavior of particle gel models. First, we defined a general class of effective interactions with 2-body and 3-body terms and used a new interparticle potential to numerically model colloidal gels at low volume fractions. We then constructed particle gel models and investigated their mechanical response under large shear deformation. We discussed the mechanical behavior in terms of the gel topology, which is directly related to the specific form of the potential. Finally, we compared the findings of the present study with those from models previously developed for the numerical analysis of colloidal gels. This comparison was done in order to highlight possible effects that a specific choice of potential formulation could have on the mechanical properties of particle gel models.

A potential with a 2-body term and a 3-body term was used to express the interaction between colloidal particles at low volume fractions. It was found that the 2-body term would influence the locality of the interactions. In particular, a long-range potential with a wide well makes the systems more prone to phase separation and requires a strong repulsive

3-body term to maintain the open structure of soft gels. On the other hand, a short-range potential with a narrow well corresponds to a diffusion-limited aggregation process. Numerical models, having an identical 2-body term, showed different network topology and mechanical response, which indicates that the formulation of the 3-body term has a strong effect on the behavior of soft gels. In particular, a potential with no preferred, or multiple, equilibrium configurations can lead to systems that are not statically determinate; performing numerical energy minimization for these systems can be very challenging. Moreover, the use of a radial modulation function in the 3-body term can cause this term to have an axial repulsive effect in the direction of the bonds in addition to its influence on the angle between neighboring bonds. Thus, the 2-body and 3-body terms cannot be directly mapped to the stretching and bending modes of deformation, respectively [52, 60].

The current study also provided microscopic explanations for the strain softening behavior of the gels under shear deformation. AQS simulations were performed in order to demonstrate that strain-softening is not solely due to rheological effects at finite temperature. To support the above statement, we computed the correlation between the stretch of interparticle bonds and their alignment in the direction of the maximum principal stress of the network. An anticorrelation was observed between these two quantities during the initial softening phase of the stress–strain behavior. This suggests that besides the release of residual bending stress (3-body term) during the straightening of curly chains, reorientation of stressed axial bonds between particles (2-body term) could play an important role in the initial softening response of low volume fraction gel models.

Finally, the numerical simulations of this work showed that topology and mechanical behavior of gels are not bounded to a single choice of effective interactions. We obtained qualitatively similar behavior and results for models whose mathematical formulation differs from each other [27, 28]. Thus, both the topology and the local mechanical interactions between colloidal particles are important in defining an appropriate potential, with a 2-body term and a 3-body term, for the mechanical response of soft gels. In the end, it is noted that although the current work was able to provide some new insight into certain aspects of the behavior of colloidal gel networks, future synergistic numerical modeling and experimental studies are required for better understanding of their behavior. Furthermore, the three gel models studied here and in literature have used specific choices of model parameters, i.e. no parametric studies have been done to demonstrate possible effects of different choices on the numerical predictions. Future studies are required to address this important drawback by investigating whether there exists a general framework for choosing model parameters and assessing their influence on numerical results. Finally, it is noted that the conclusions of the present work are primary valid for the interaction potential proposed here, i.e. different mechanics and microstructure may be seen if other potential functions [29] are used.

Acknowledgment

ORCID iDs

Hamed Hatami-Marbini ⬤ https://orcid.org/0000-0002-6693-2121

References

[1] Sacanna S *et al* 2013 Shaping colloids for self-assembly *Nat. Commun.* **4** 1
[2] Sacanna S *et al* 2010 Lock and key colloids *Nature* **464** 575–8
[3] Wang Y *et al* 2012 Colloids with valence and specific directional bonding *Nature* **491** 51–5
[4] Chen Q, Bae S C and Granick S 2011 Directed self-assembly of a colloidal kagome lattice *Nature* **469** 381–4
[5] Bannwarth M B *et al* 2015 Colloidal polymers with controlled sequence and branching constructed from magnetic field assembled nanoparticles *ACS Nano* **9** 2720–8
[6] Bannwarth M and Crespy D 2014 Combining the best of two worlds: nanoparticles and nanofibers *Chem. Asian J.* **9** 2030–5
[7] Demortiere A *et al* 2014 Self-assembled tunable networks of sticky colloidal particles *Nat. Commun.* **5** 1
[8] Grzelczak M *et al* 2010 Directed self-assembly of nanoparticles *ACS Nano* **4** 3591–605
[9] Stokes J R and Frith W J 2008 Rheology of gelling and yielding soft matter systems *Soft Matter* **4** 1133
[10] Lu P J and Weitz D A 2013 Colloidal particles: crystals, glasses, and gels *Ann. Rev. Condens. Matter Phys.* **4** 217–33
[11] Tanaka H, Nishikawa Y and Koyama T 2005 Network-forming phase separation of colloidal suspensions *J. Phys.: Condens. Matter* **17** L143–53
[12] Segrè P *et al* 2001 Glasslike kinetic arrest at the colloidal-gelation transition *Phys. Rev. Lett.* **86** 6042–5
[13] Kohl M *et al* 2016 Directed percolation identified as equilibrium pre-transition towards non-equilibrium arrested gel states *Nat. Commun.* **7** 11817
[14] Capellmann R F *et al* 2016 Structure of colloidal gels at intermediate concentrations: the role of competing interactions *Soft Matter* **12** 9303–13
[15] Lu P J *et al* 2008 Gelation of particles with short-range attraction *Nature* **453** 499–503
[16] Dinsmore A D *et al* 2006 Microscopic structure and elasticity of weakly aggregated colloidal gels *Phys. Rev. Lett.* **96** 1
[17] Pantina J P and Furst E M 2005 Elasticity and critical bending moment of model colloidal aggregates *Phys. Rev. Lett.* **94** 1
[18] Dinsmore A D and Weitz D A 2002 Direct imaging of three-dimensional structure and topology of colloidal gels *J. Phys.: Condens. Matter* **14** 7581–97
[19] Lazzari S *et al* 2016 Fractal-like structures in colloid science *Adv. Colloid Interface Sci.* **235** 1–13
[20] Santos P H S, Campanella O H and Carignano M A 2010 Brownian dynamics study of gel-forming colloidal particles *J. Phys. Chem.* B **114** 13052–8
[21] Dickinson E 2013 Structure and rheology of colloidal particle gels: Insight from computer simulation *Adv. Colloid Interface Sci.* **199–200** 114–27
[22] Blaak R, Miller M A and Hansen J-P 2007 Reversible gelation and dynamical arrest of dipolar colloids *Europhys. Lett.* **78** 26002
[23] Gado E D and Kob W 2010 A microscopic model for colloidal gels with directional effective interactions: network induced glassy dynamics *Soft Matter* **6** 1547
[24] Gado E D and Kob W 2007 Length-scale-dependent relaxation in colloidal gels *Phys. Rev. Lett.* **98** 1
[25] Zaccarelli E *et al* 2005 Model for reversible colloidal gelation *Phys. Rev. Lett.* **94** 1–4
[26] Sciortino F and Zaccarelli E 2011 Reversible gels of patchy particles *Curr. Opin. Solid State Mater. Sci.* **15** 246–53
[27] Saw S *et al* 2009 Structural relaxation of a gel modeled by three body interactions *Phys. Rev. Lett.* **103** 1
[28] Colombo J, Widmer-Cooper A and Gado E D 2013 Microscopic picture of cooperative processes in restructuring gel networks *Phys. Rev. Lett.* **110** 1
[29] Zaccarelli E 2007 Colloidal gels: equilibrium and non-equilibrium routes *J. Phys.: Condens. Matter* **19** 323101
[30] Baxter R 1968 Percus–Yevick equation for hard spheres with surface adhesion *J. Chem. Phys.* **49** 2770–4
[31] Bouzid M and Gado E D 2017 Network topology in soft gels: hardening and softening materials *Langmuir* **34** 773–81
[32] Bouzid M *et al* 2017 Elastically driven intermittent microscopic dynamics in soft solids *Nat. Commun.* **8** 15846
[33] Dibble C J, Kogan M and Solomon M J 2008 Structural origins of dynamical heterogeneity in colloidal gels *Phys. Rev.* E **77** 1
[34] Stillinger F H and Weber T A 1985 Computer simulation of local order in condensed phases of silicon *Phys. Rev.* B **31** 5262–71
[35] Vink R L C *et al* 2001 Fitting the Stillinger–Weber potential to amorphous silicon *J. Non-Cryst. Solids* **282** 248–55
[36] Molinero V, Sastry S and Angell C A 2006 Tuning of tetrahedrality in a silicon potential yields a series of monatomic (metal-like) glass formers of very high fragility *Phys. Rev. Lett.* **97** 1
[37] Zhang Z, Chen Y and Zheng H 2014 A modified Stillinger} Weber potential-based hyperelastic constitutive model for nonlinear elasticity *Int. J. Solids Struct.* **51** 1542–54
[38] Saw S *et al* 2011 Computer simulation study of the phase behavior and structural relaxation in a gel-former modeled by three-body interactions *J. Chem. Phys.* **134** 164506
[39] Colombo J and Gado E D 2014 Stress localization, stiffening, and yielding in a model colloidal gel *J. Rheol.* **58** 1089–116
[40] Colombo J and Gado E D 2014 Self-assembly and cooperative dynamics of a model colloidal gel network *Soft Matter* **10** 4003
[41] Plimpton S 1995 Fast parallel algorithms for short-range molecular dynamics *J. Comput. Phys.* **117** 1–19
[42] Tanguy A *et al* 2002 Continuum limit of amorphous elastic bodies: a finite-size study of low-frequency harmonic vibrations *Phys. Rev.* B **66** 1
[43] Maloney C E and Lemaître A 2006 Amorphous systems in athermal, quasistatic shear *Phys. Rev.* E **74** 1
[44] Thompson A P, Plimpton S J and Mattson W 2009 General formulation of pressure and stress tensor for arbitrary many-body interaction potentials under periodic boundary conditions *J. Chem. Phys.* **131** 154107
[45] Storm C *et al* 2005 Nonlinear elasticity in biological gels *Nature* **435** 191–4
[46] Keshavarz B *et al* 2017 Nonlinear viscoelasticity and generalized failure criterion for polymer gels *ACS Macro Lett.* **6** 663–7
[47] Hatami-Marbini H and Picu R C 2008 Scaling of nonaffine deformation in random semiflexible fiber networks *Phys. Rev.* E **77** 1

[48] Hatami-Marbini H and Picu R C 2009 Effect of fiber orientation on the non-affine deformation of random fiber networks *Acta Mech.* **205** 77–84

[49] Heussinger C and Frey E 2006 Floppy modes and nonaffine deformations in random fiber networks *Phys. Rev. Lett.* **97** 105501

[50] Zaccone A and Scossa-Romano E 2011 Approximate analytical description of the nonaffine response of amorphous solids *Phys. Rev.* B **83** 184205

[51] Amann C P *et al* 2013 Overshoots in stress–strain curves: colloid experiments and schematic mode coupling theory *J. Rheol.* **57** 149–75

[52] Broedersz C P and MacKintosh F C 2014 Modeling semiflexible polymer networks *Rev. Mod. Phys.* **86** 995–1036

[53] Hatami-Marbini H 2016 Scaling properties of three-dimensional random fibre networks *Phil. Mag. Lett.* **96** 165–74

[54] Hatami-Marbini H 2016 Nonaffine behavior of three-dimensional semiflexible polymer networks *Phys. Rev.* E **93** 1

[55] Janmey P A *et al* 2006 Negative normal stress in semiflexible biopolymer gels *Nat. Mater.* **6** 48–51

[56] Xu D, Liu C-Y and Craig S L 2011 Divergent shear thinning and shear thickening behavior of supramolecular polymer networks in semidilute entangled polymer solutions *Macromolecules* **44** 2343–53

[57] Kim O V *et al* 2014 Structural basis for the nonlinear mechanics of fibrin networks under compression *Biomaterials* **35** 6739–49

[58] Feng D *et al* 2018 Disease-causing mutation in α -actinin-4 promotes podocyte detachment through maladaptation to periodic stretch *Proc. Natl Acad. Sci.* **115** 1517–22

[59] Tabatabai A P, Kaplan D L and Blair D L 2015 Rheology of reconstituted silk fibroin protein gels: the epitome of extreme mechanics *Soft Matter* **11** 756–61

[60] Hatami-Marbini H and Picu C R 2012 Modeling the mechanics of semiflexible biopolymer networks: non-affine deformation and presence of long-range correlations *Advances in Soft Matter Mechanics* (Berlin: Springer) pp 119–45

[61] Hatami-Marbini H and Shriyan V 2017 Topology effects on nonaffine behavior of semiflexible fiber networks *Phys. Rev.* E **96** 1

[62] Hatami-Marbini H 2018 Simulation of the mechanical behavior of random fiber networks with different microstructure *Eur. Phys. J.* E **41** 1

[63] Licup A J *et al* 2015 Stress controls the mechanics of collagen networks *Proc. Natl Acad. Sci.* **112** 9573–8

[64] Zaccone A, Schall P and Terentjev E M 2014 Microscopic origin of nonlinear nonaffine deformation in bulk metallic glasses *Phys. Rev.* B **90** 140203

[65] Laurati M *et al* 2017 Long-lived neighbors determine the rheological response of glasses *Phys. Rev. Lett.* **118** 018002